



**HAL**  
open science

## A facile fabrication of dissolving microneedles containing 5-aminolevulinic acid

Mathilde Champeau, Dorothée Jary, Laurent Mortier, Serge Mordon, Séverine Vignoud

► **To cite this version:**

Mathilde Champeau, Dorothée Jary, Laurent Mortier, Serge Mordon, Séverine Vignoud. A facile fabrication of dissolving microneedles containing 5-aminolevulinic acid. *International Journal of Pharmaceutics*, 2020, 586, pp.119554 -. 10.1016/j.ijpharm.2020.119554 . hal-03492052

**HAL Id: hal-03492052**

**<https://hal.science/hal-03492052>**

Submitted on 18 Jul 2022

**HAL** is a multi-disciplinary open access archive for the deposit and dissemination of scientific research documents, whether they are published or not. The documents may come from teaching and research institutions in France or abroad, or from public or private research centers.

L'archive ouverte pluridisciplinaire **HAL**, est destinée au dépôt et à la diffusion de documents scientifiques de niveau recherche, publiés ou non, émanant des établissements d'enseignement et de recherche français ou étrangers, des laboratoires publics ou privés.



Distributed under a Creative Commons Attribution - NonCommercial 4.0 International License

## A facile fabrication of dissolving microneedles containing 5-aminolevulinic acid.

Mathilde Champeau<sup>a,b,\*</sup>, Dorothee Jary<sup>a</sup>, Laurent Mortier<sup>b</sup>, Serge Mordon<sup>b</sup>, Séverine Vignoud<sup>a</sup>

<sup>a</sup>CEA, LETI-DTBS, 17 rue des Martyrs, Grenoble Cedex, France

<sup>b</sup>Univ. Lille, Inserm, CHU Lille, U1189 - ONCO-THAI - Assisted Laser Therapy and Immunotherapy for Oncology, F-59000 Lille, France

---

### Abstract

Photodynamic therapy induced by protoporphyrin IX (PpIX) is widely used to treat precancerous skin lesions. The penetration depth of the prodrug 5-aminolevulinic acid (5-ALA) using topical application is currently limited, which hampers the production of PpIX in deep seated lesions. To enhance 5-ALA delivery in deep skin layers, a soluble microneedles patch (MN-patch) containing 5-ALA has been successfully developed by using a fast solvent casting molding method which could be easily up-scaled. The shape, number and height of the needles have been designed according to the medical application and the mechanical strain necessary for skin insertion. Hyaluronic acid (HA) has been chosen as the needle materials due to its biocompatibility, fast solubility and biodegradation and was mixed with 5-ALA prior to casting. HA-based MN-patch containing 5-ALA have exhibited mechanical properties enabling a good insertion into the skin without significant damages to MN. Interactions between HA and 5-ALA were evaluated by Fourier transform infrared spectroscopy (FTIR) and carbon nuclear magnetic resonance (<sup>13</sup>C NMR), stability of 5-ALA in the MN-patch was monitored by proton nuclear magnetic resonance (<sup>1</sup>H NMR) and exhibited a good stability over 5 months after manufacturing. Dissolution rate of the whole patch was completed in 1 hour in *ex vivo* rat skin without cytotoxicity. Overall, the MN-patch can be a promising technique to enhance 5-ALA penetration and produce PpIX in deeper skin lesions.

**Keywords:** 5-aminolevulinic acid, hyaluronic acid, dissolving microneedles, solvent casting molding method, photodynamic therapy

---

\*Corresponding author

Email address: [mathilde.champeau@cea.fr](mailto:mathilde.champeau@cea.fr) (Mathilde Champeau )

## Glossary

- <sup>13</sup>C NMR** carbon nuclear magnetic resonance. 1, 7, 8, 13, 14
- <sup>1</sup>H NMR** proton nuclear magnetic resonance. 1, 7, 10, 14
- 5-ALA** 5-aminolevulinic acid. 1–4, 6–17, 21–24
- 5 **FTIR** Fourier transform infrared spectroscopy. 1, 7, 12
- HA** hyaluronic acid. 1, 3, 4, 6, 7, 9–15, 21, 22
- MN** microneedle. 2–4, 6, 7, 17
- MN<sub>l</sub>** little microneedle. 4, 5, 9, 16–22, 24
- MN<sub>t</sub>** tall microneedle. 4, 5, 9, 11, 17, 19–22, 24
- 10 **MN-patch** microneedles patch. 1, 4, 9, 11, 21, 23
- PDMS** polydimethylsiloxane. 4–6
- PDT** photodynamic therapy. 1–4, 12, 15, 24
- PpIX** protoporphyrin IX. 1, 2, 24
- PY** 2,5-pyrazinedipropionic acid. 4, 7, 8, 12, 14, 15, 22–24
- 15 **RT** room temperature. 3
- SC** *stratum corneum*. 2, 16, 24
- TGA** thermogravimetric analysis. 6, 11, 15

## 1. Introduction

Transdermal drug delivery, usually ensured by using creams, lotion or patches, offers several  
20 important advantages over traditional drug delivery methods (oral administration or injection).  
It indeed enables to control the amount of drug delivered at local areas, which allows to admin-  
istrate lower doses [1]. A targeted drug administration also decreases undesirable side effects  
and increases therapeutic benefits [2]. Moreover the non-invasive nature of transdermal drug  
delivery allows to improve patient acceptability and compliance [3]. This way of administra-  
25 tion is commonly used for the treatment of skin cancers by photodynamic therapy (PDT) by  
using creams. PDT is a treatment relying on a combination of three parameters: drug content,  
oxygenation rate and light irradiation intensity. 5-aminolevulinic acid (5-ALA) is widely used  
as a PpIX photosensitive precursor and topically applied on the skin lesions. Light irradiation  
at PpIX exciting wavelength combined with the presence of oxygen promotes photochemical  
30 reaction leading to cell death. Treatment efficiency is linked to different factors including drug  
penetration. However, drug penetration is often hampered by the *stratum corneum* (SC), which  
is the outer first layer of epidermis that provides a barrier to external environment and difficult  
to penetrate for many drugs [3]. Moreover, the physicochemical properties of 5-ALA such as its  
hydrophilicity or zwitterionic nature also limit its penetration, which prevents access to deep skin  
35 layers [4, 5]. These limitations make PDT unsuitable for basal cell carcinoma (superficial, nodu-  
lar or infiltrative) and invasive squamous cell carcinoma that have tumor cells in deep epidermis  
or dermis [6, 7]. To overcome this lack of drug penetration, different (chemical or physical)  
strategies have been suggested [5], among which the use of microneedles (MNs) appears to be a  
promising technique [8–10].

40 MNs are assembled together to form an array or patch that enables to bypass the SC by creat-  
ing holes in it, resulting in enhanced transdermal drug delivery through the created microchannels  
[11]. MNs have been developed with a height inferior to 900  $\mu\text{m}$  in order to limit pain. Indeed,  
this height criterion improves patient compliance and safety since MN cannot penetrate deep  
vascular and nervous regions. At the same time, this height is adequate to successfully reach  
45 the dermal layers without inducing bleeding and touching active immune cells. Due to their  
microsize, MN cannot be seen by patients, which reduces needle phobia [12]. Although MN  
dimensions are in the microscale, their design with adequate materials confers them strong me-  
chanical properties to pierce the SC, which allows the diffusion in skin tissues of hydrophilic or  
high molecular weight drugs [13].

50 Different types of MN-mediated drug delivery have been developed. Solid MNs can be inserted  
in the skin and then removed letting micron-scale pores in the skin surface, followed by drug  
formulation application. This passive diffusion of drugs requires a two-step application process,  
which is prone to errors in the delivered dose [14]. It also can be dangerous for the patient itself  
since materials used to produce solid MNs such as silicon have dubious biocompatibility and  
55 can break, which could lead to complications [15, 16]. To avoid the two-step application, drugs  
have been coated on solid MNs. Nevertheless, the drugs were rapidly delivered in small quantity  
( $\leq 2$  mg) [11, 17, 18] and the risk of broken materials was still present. Hollow MNs are another  
type of MN whose principle is based on hypodermic needles. Such MNs could avoid the two-step  
process and deliver a large drug amount but due to their micro size they may become blocked  
60 by compressed dermal tissue when inserted into the skin [11].

Recently, dissolving MNs have been attracting attention for drug delivery since they allow to  
get rid of the aforementioned issues. The principle is that a drug is encapsulated in the needle  
matrix that is biocompatible, soluble and mechanically robust. When inserted in the skin, this  
matrix is dissolved by body fluids and delivers the drug with a controlled kinetic profile depending  
65 on the chosen matrix. Materials used as matrix are often polymers, such as carbohydrates  
[19, 20] or other bio-sourced components [16]. Polymers such as polyvinylpyrrolidone [21] or  
carboxymethylcellulose [20, 22] allow a rapid dissolution ( $\leq 5$  min or  $\leq 20$  min, respectively)  
whereas polylactic acid or poly(lactic-co-glycolic acid) are biodegraded in a few days [23, 24].  
Because the drug is embedded in the polymer matrix, the fabrication process must be soft to  
70 ensure drug stability and avoid as much as possible the use of organic solvents.

Hyaluronic acid (HA) is a polysaccharide that can be shape-molded and stored at room  
temperature (RT). HA is a component naturally present in the human body, widely distributed  
in body tissues, intracellular fluids and well excreted by different organs ; it is a polymer fully  
biocompatible and already used in many medical fields [25]. Moreover, this is a water soluble  
75 polymer that can be dissolved after skin contact in a few minutes ( $\leq 10$  min) [26, 27]. These  
characteristics make it a good candidate to produce dissolving MNs to transport 5-ALA.

In the present study, we aimed at exploring the processing and the properties of HA-MN  
with 5-ALA embedded in the polymer matrix. 5-ALA was embedded only in one easy step, in  
the whole patch including the basis without MN. The aim was to deliver 5-ALA from the top of  
80 the skin to the deeper skin lesions to allow PDT treatment on the whole damaged skin volume.  
Since 5-ALA and HA were mixed together, interactions between the polymer and the drug was  
carefully studied and 5-ALA stability was investigated for different time periods. Furthermore,

microneedles shape was designed as a “pencil-tip” to confer them strong mechanical properties to penetrate the cutaneous lesions. As all basal cell carcinomas do not extend to the same depth, different heights of needles were processed and characterized. Moreover MN-patch could be loaded with large different amounts of 5-ALA which offer different dosages. The characteristics of the MN-patch (compression, insertion tests, dissolution rate) have been conducted to evaluate whether this strategy is a promising approach to enhance PDT outcomes on deep skin cancers.

## 2. Materials and methods

### 2.1. Chemicals

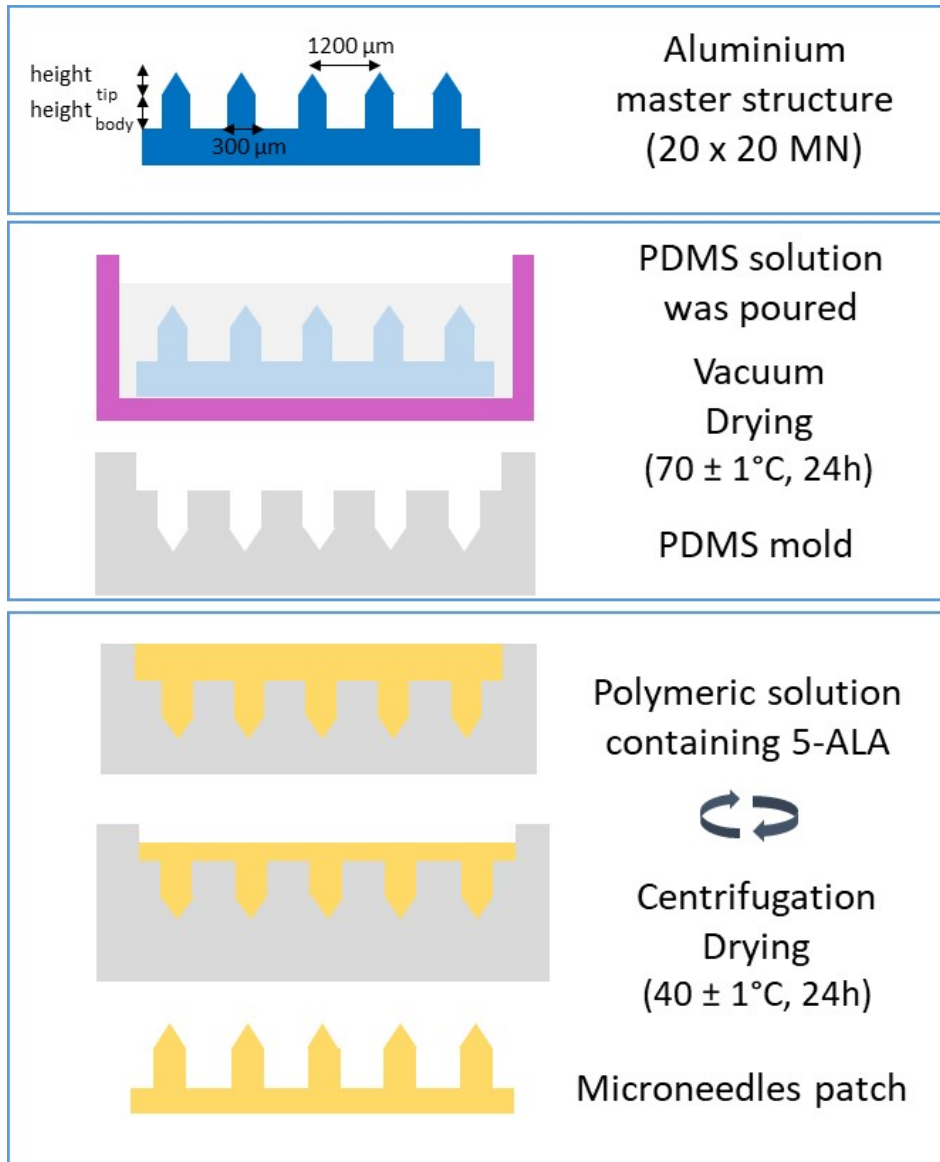
5-ALA hydrochloride salt (GMP grade) was purchased from Biosynth Chemistry & Biology. Polydimethylsiloxane (PDMS) (Sylgard , Dow Corning), potassium phthalate monobasic (KHP, TraceCERT®), Dulbecco’s modified eagle medium (DMEM), penicillin streptomycin solution (Pen Strep) and the cell proliferation reagent WST-1 were obtained from Sigma-Aldrich Chemical Co. HA with a molecular weight (MW) of  $(5.50 \pm 0.04) \times 10^4 \text{ g mol}^{-1}$  was purchased from Contipro France. 2,5-pyrazinedipropionic acid (PY) was purchased from Carbosynth Product. All other chemicals were of analytical reagent grade.

### 2.2. Fabrication of HA microneedles patches

Soluble HA microneedles were fabricated by solvent casting molding method. This technique consists of using an aluminium master structure to obtain a PDMS mold from which dissolvable polymer microneedle replicates are formed. The overall steps of the preparation of dissolving microneedles are displayed in scheme 1.

#### • Aluminum master structure

An array of  $20 \times 20$  MN was machined on an aluminium surface of  $25 \times 25 \text{ mm}^2$ . MN design is similar to a pencil-tip: a conical tip sits on top of a cylinder body. Two types of MN were designed: a tall one ( $MN_t$ ) and a little one ( $MN_l$ ). For the tall microneedle patch, the height was  $750 \mu\text{m}$  ( $height_{tip} = 300 \mu\text{m}$  and  $height_{body} = 450 \mu\text{m}$ ), the base diameter was  $300 \mu\text{m}$  and each MN was tip-spaced with  $1200 \mu\text{m}$ . For the little microneedle patch, the height was  $400 \mu\text{m}$  ( $height_{tip} = 150 \mu\text{m}$  and  $height_{body} = 250 \mu\text{m}$ ), base diameter was  $300 \mu\text{m}$  and each MN was tip-spaced with  $1200 \mu\text{m}$ .



Scheme 1: Preparation of the MN-patch by solvent casting molding method. Three major steps are essential: aluminium master structure design, fabrication of PDMS mold and casting of the solution in the mold. Two heights were designed for the aluminium master structure: a tall one  $MN_t$  at 750 µm and a little one  $MN_l$  at 400 µm.

- **PDMS mold**

A PDMS solution (10% reticulated) was poured on the master structure tipped up, then vacuum was applied and PDMS was dried at  $(70 \pm 1)^\circ\text{C}$  for 24 h.

115 • **Molding of HA microneedles**

A HA solution ( $50 \text{ mg mL}^{-1}$ ) was prepared by vigorous mixing in distilled water and different amounts of 5-ALA were added to the solution leading to final concentrations of 0, 10 or  $50 \text{ mg mL}^{-1}$ .  $200 \mu\text{L}$  of HCl at  $0.03 \text{ mol L}^{-1}$  were added to the solution in order to be at *pH* of 5 and ensure 5-ALA stability. A solution amount of  $2.0 \text{ mL}$  was casted in the PDMS mold. The mold was centrifugated at  $21 \text{ }^\circ\text{C}$  and  $4000 \text{ rpm}$  for  $35 \text{ min}$  to ensure a complete filling of the cavities. Then it was placed in an oven at  $(40 \pm 1) \text{ }^\circ\text{C}$  for  $24 \text{ h}$ , after which the HA microneedle patch was gently removed from the mold. Each patch is expected to contain  $100 \text{ mg}$  of HA and  $0 \text{ mg}$  (MN-0),  $20 \text{ mg}$  (MN-20) or  $100 \text{ mg}$  (MN-100) of 5-ALA.

120 *2.3. Characterization of 5-ALA-MN-patch*

125 *2.3.1. Microscopic analysis of HA microneedle arrays*

A digital microscope (VHX 8000, Keyence) was used to observe the morphology (height, tip diameter, width of base) of microneedle patch under normal light. Microneedles heights were analyzed with the ImageJ software.

*2.3.2. Mechanical properties*

130 To determine the loss in height of MN when compressed at a precise force, a texturometer (TA.XT Plus, Stable micro systems, UK) was used. The MN array was placed on the metal platform and an axial compression force was applied with the probe. The MN array was pressed at a rate of  $0.5 \text{ mm s}^{-1}$  with a force ranging from  $0 \text{ N}$  per needle to  $0.5 \text{ N}$  per needle for  $10 \text{ s}$ . Pre-test and post-test speed were of  $5 \text{ mm s}^{-1}$ , and the trigger force was set at  $0.01 \text{ N}$ . The patch  
135 was then observed under digital microscope and measurements were performed with the ImageJ software.

*2.3.3. Water content in the microneedle patch*

To evaluate the residual water content in the microneedle patch, thermogravimetric analysis (TGA) was performed at a heating rate of  $5 \text{ }^\circ\text{C}/\text{min}$  on a TGA Q5000 from TA Instruments and  
140 TA universal analysis was the software used.

*2.4. Drug stability in the MN patch*

*2.4.1. Chemical stability of 5-ALA by quantitative proton nuclear magnetic resonance ( $^1\text{H}$  NMR)*

To evaluate the amount of 5-ALA in the MN-patch, potassium phthalate monobasic (KHP) was added as an internal standard. A solution of KHP was prepared at  $10 \text{ mg mL}^{-1}$  in  $\text{D}_2\text{O}$ .

145 For analysis, a small amount of the MN-patch (approximately 10 mg) was dissolved in 650  $\mu\text{L}$  of  $\text{D}_2\text{O}$  and 50  $\mu\text{L}$  of the KHP solution was added. Then proton nuclear magnetic resonance spectra were recorded using a Bruker Spectrospin spectrometer operating at 300 MHz and 295 K. The TopSpin software was used to analyze the spectra. The content of 5-ALA was calculated using one of the signals of the internal KHP standard and one of the signals of the analyte as presented  
 150 in equation 1, where  $x$  represents the analyte 5-ALA,  $NH_{\text{KHP}}$  is the number of protons of KHP (2),  $NH_x$  is the number of protons of 5-ALA (2),  $m_{\text{KHP}}$  is the weighted amount of standard material potassium phthalate monobasic,  $Mw_x$  is the molar weight of 5-ALA ( $131.13 \text{ g mol}^{-1}$ ),  $Mw_{\text{KHP}}$  is the molar weight of KHP ( $204.22 \text{ g mol}^{-1}$ ),  $A_x$  is the integral between 4.0 and 4.15 ppm and  $A_{\text{KHP}}$  is the integral between 7.45 and 7.6 ppm.

$$m_x = \frac{NH_{\text{KHP}} \times m_{\text{KHP}} \times Mw_x \times A_x}{NH_x \times Mw_{\text{KHP}} \times A_{\text{KHP}}} \quad (1)$$

155 The same equation 1 was also used to quantify the amount of the degradation product of 5-ALA, which is 2,5-pyrazinedipropionic acid (PY). When the analyte is PY,  $NH_x$  is equal to 2,  $Mw_x$  is  $224.21 \text{ g mol}^{-1}$  and  $A_x$  is the integral between 8.35 and 8.45 ppm.

The weight percentages of 5-ALA and PY were then obtained according to equations 2 and 3, respectively, where  $m_{5-ALA}$  and  $m_{PY}$  are calculated by equation 1 and  $m_{tot}$  corresponds to  
 160 the mass of the MN-patch (either MN-20 or MN-100) used for the analysis.

$$w_{5-ALA} = \frac{m_{5-ALA}}{m_{tot}} \quad (2)$$

$$w_{PY} = \frac{m_{PY}}{m_{tot}} \quad (3)$$

#### 2.4.2. Interactions between drug and polymer followed by FTIR and $^{13}\text{C}$ NMR

Molecular interactions between 5-ALA and HA in the MN-patch were studied with ATR-FTIR. FTIR spectra of the MN patch were performed using a spectrometer IRAffinity-1, MIRacle-10 from Shimadzu in the wave number range from 500 to  $5000 \text{ cm}^{-1}$  with a resolution of  $4 \text{ cm}^{-1}$ .  
 165 Samples were directly placed on the crystal surface and scanned 32 times per analysis.

To determine the chemical structure of hyaluronic acid, analysis of the  $^{13}\text{C}$  nucleus present in the compound was studied by  $^{13}\text{C}$  NMR spectroscopy. Approximately ten milligrams of HA was dissolved in 700  $\mu\text{L}$  of  $\text{D}_2\text{O}$ . A DEPT-Q (Distorsionless enhancement by polarization transfer including the detection of quaternary nuclei) sequence was performed to complete carbon

170 assignments using a Bruker Spectrospin spectrometer operating at 75 MHz, 355 K and using a  
5 mm QNP probe.

## 2.5. Penetration and dissolution of the microneedles patch

### 2.5.1. Skin model

As an alternative to biological tissue, a modeling clay (Plastiline  $\text{\textcircled{R}}$ , composed of kaolin,  
175 sulfur and glycerine) was spread to obtain a thickness of 2 cm and used as a skin model regard-  
ing mechanical properties. Microneedle patches (MN-0, MN-20 and MN-100) were inserted in  
this phantom skin by thumb pressure that is estimated to be at 0.17 N/needle (measurement  
performed with the texturometer) and then was removed. The skin model was observed with a  
digital microscope to evaluate the penetration profile and depth.

### 180 2.5.2. *Ex vivo* rat skin

*Ex vivo* rat skin was stretched and fixed with pins on a polystyrene plate. MN-patches were  
inserted in the *ex vivo* rat skin by thumb pressure. The pressure was kept constant for 10 sec.  
Then the MN-patch was kept inserted in the skin for a precise amount of time (from 5 min  
to 45 min) with the help of an occlusive tape (Tegaderm<sup>TM</sup>, 3M). After MN-patch removal, the  
185 skin was observed in top view and then it was embedded in tissue freezing medium (TFM, M-M  
FRANCE). As for the MN-patch, it was kept in a dry Petri dish until microscope analysis was  
carried out to quantify the dissolution kinetics.

## 2.6. Drug release measurements

Petri dishes (surface: 9.6 cm<sup>2</sup>) were filled with 750  $\mu$ L of water acidified with HCl to obtain  
190 a *pH* of 5. Therefore, a thin water layer (< 1 mm) was present in all the Petri dishes. Then  
MN-patches loaded with 5-ALA, either MN-20 or MN-100, were placed needles down into the  
Petri dishes and slightly agitated at 75 rpm. At predetermined time points, the solution was  
collected for analysis and replaced by a same volume of fresh water at *pH*5. The amount of  
solution removed was freeze dried for 72 h and then dispersed in D<sub>2</sub>O for quantifying released  
195 5-ALA by <sup>1</sup>H NMR according to the previous equations hereinbelow. The experiments were  
conducted in triplicate.

## 2.7. *In vitro* cytotoxicity study

The cytotoxicity of MN-patches as well as individual products, 5-ALA, 5-ALA-free patches  
(MN-0) and product of 5-ALA biodegradation (PY), was assessed. To this end, the patches

200 or pure chemicals were dissolved in cell culture media. After 24 h of preincubation of the cells (NIH3T3 murine fibroblasts cells,  $4 \times 10^3 \text{ cells/well}$ ) in DMEM containing 10% of new born calf serum and 1% of Pen Strep, the medium was replaced by one containing the different tested products followed by a new incubation of 24 h at 37 °C. The WST-1 reagent was then added. After 2 h at 37 °C, absorbance at 450 nm was recorded using a microplate reader (Infinite 205 M1000, Tecan). The absorbance was linked to the metabolic activity of cell mitochondria and the density of living cells (DLC) was calculated as mentioned in equation 4, where AS, APC and ANC respectively represent the absorbances of the sample, the positive control and the negative control, the negative control being cells growing in the culture media without any added product and the positive control being cells growing in the cell culture media containing 210  $\text{H}_2\text{O}_2$  at  $0.01 \text{ mol L}^{-1}$ .

$$DLC = \frac{AS - APC}{ANC - APC} \times 100 \quad (4)$$

### 3. Results and discussion

#### 3.1. Microneedle preparation and characterizations

Tall microneedle ( $MN_t$ ) and little microneedle ( $MN_l$ ) were successfully produced with expected dimensions using the solvent casting molding method as displayed in figure 1. The heights 215 of the  $MN_t$  and  $MN_l$  microneedles were respectively  $749 \pm 6 \mu\text{m}$  and  $390 \pm 7 \mu\text{m}$  and the base diameter was  $285 \pm 10 \mu\text{m}$  which corresponds well to the original master structure dimensions. The slight difference in microneedle height (respectively 0.13% and 2.5% for  $MN_t$  and  $MN_l$ ) and diameter (5%) might be explained by the retraction of the HA matrix during the drying process. Mönkäre et al. also reported a height reduction of 6.6% when they developed immunoglobulinG- 220 loaded hyaluronan-based dissolving microneedles by solvent casting molding method and they explained it by the shrinking of the HA during drying process [27]. Similarly Zhao et al. fabricated 5-ALA-loaded dissolving microneedles made of HA and attribute the 9.3% reduction in height to water evaporation during drying process [28] which could consequently induce polymer shrinkage.

225 Drug distribution was expected to be homogeneous as the solution containing 5-ALA and HA was homogeneous before pouring. Indeed, a uniform pale yellow color could be observed from the tip to the base of the MN-patch containing 5-ALA (Figure 1, right). However, crystallization or precipitation of 5-ALA could have taken place during drying, leading to inhomogeneous drug

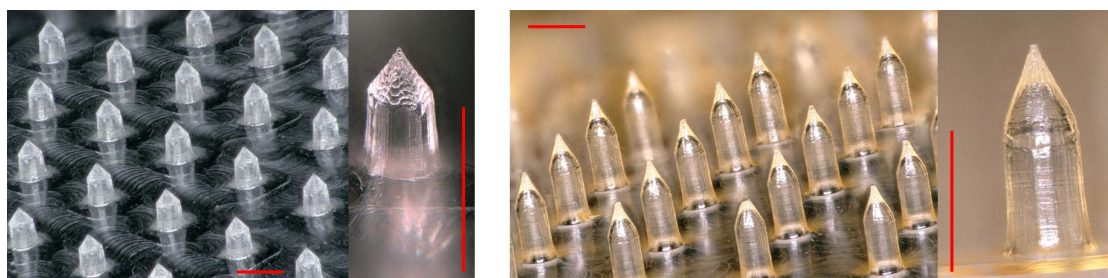


Figure 1: Digital microscopy images of MN-patch fabricated by solvent casting molding method. (Left:  $MN_t-0$ , right:  $MN_t-20$ .) Scale bars represent  $500\ \mu\text{m}$ .

distribution. Consequently analysis of 9 different parts of the patch was performed in order to  
 230 quantify drug content in each part. Each piece was analyzed by  $^1\text{H}$  NMR (Figure 2) and the  
 percentage of 5-ALA was calculated according to  $^1\text{H}$  NMR equations (Eq 1 and Eq 2).

The theoretical values for the 5-ALA relative weight percentage, considering only dry matters,  
 are respectively equal to  $17\%(\text{w/w})$  and  $50\%(\text{w/w})$  for MN-20 and MN-100. Taking into account  
 the residual water, a lower 5-ALA absolute weight percentage is expected. Indeed, the results  
 235 presented in figure 3 show that the absolute percentage of 5-ALA was of  $10.0\%(\text{w/w})$  and  
 $31.2\%(\text{w/w})$  for MN-20 and MN-100, with low intra and inter patches standard deviations ( $< 2\%$   
 $(\text{w/w})$ ) demonstrating the homogeneous distribution of the drug. For the MN-20 patch, the  
 content in water was evaluated at  $14\%(\text{w/w})$  by TGA corresponding to a drop of the 5-ALA  
 weight percentage from  $17\%(\text{w/w})$  to  $14\%(\text{w/w})$ , which is in good agreement with the obtained  
 240 value of  $10.0\%(\text{w/w})$  taking into account all the experimental errors.

The process investigated in this study allows to produce reproducible MN-patches with precise  
 amount of drug homogeneously distributed in the whole patch. Moreover, the amount of 5-ALA  
 loaded in the MN-patch was a thousand times more important than previous studies lead by  
 Zhao et al. or Zhu et al. since both authors only added 5-ALA in the tips of the HA-microneedles  
 and not in the whole needle [28, 29]. Therefore they were forced to process the microneedles in  
 245 several steps whereas performing a unique easy solvent casting method as presented in section  
 2.2 simplifies the process which would be an important asset for industrialization. Even when  
 the active component is mixed with the polymer solution, several steps may be involved. It  
 was the case for Mönkäre et al. that applied vacuum prior to centrifugation to produce IgG-  
 250 loaded hyaluronan-based dissolving microneedles[27]. For the MN-patches developed in this  
 study, centrifugation was sufficient to ensure the complete filling of all microneedle tips as the  
 poured solution at a low HA concentration ( $50\ \text{mg mL}^{-1}$ ) had a moderate viscosity with a shear

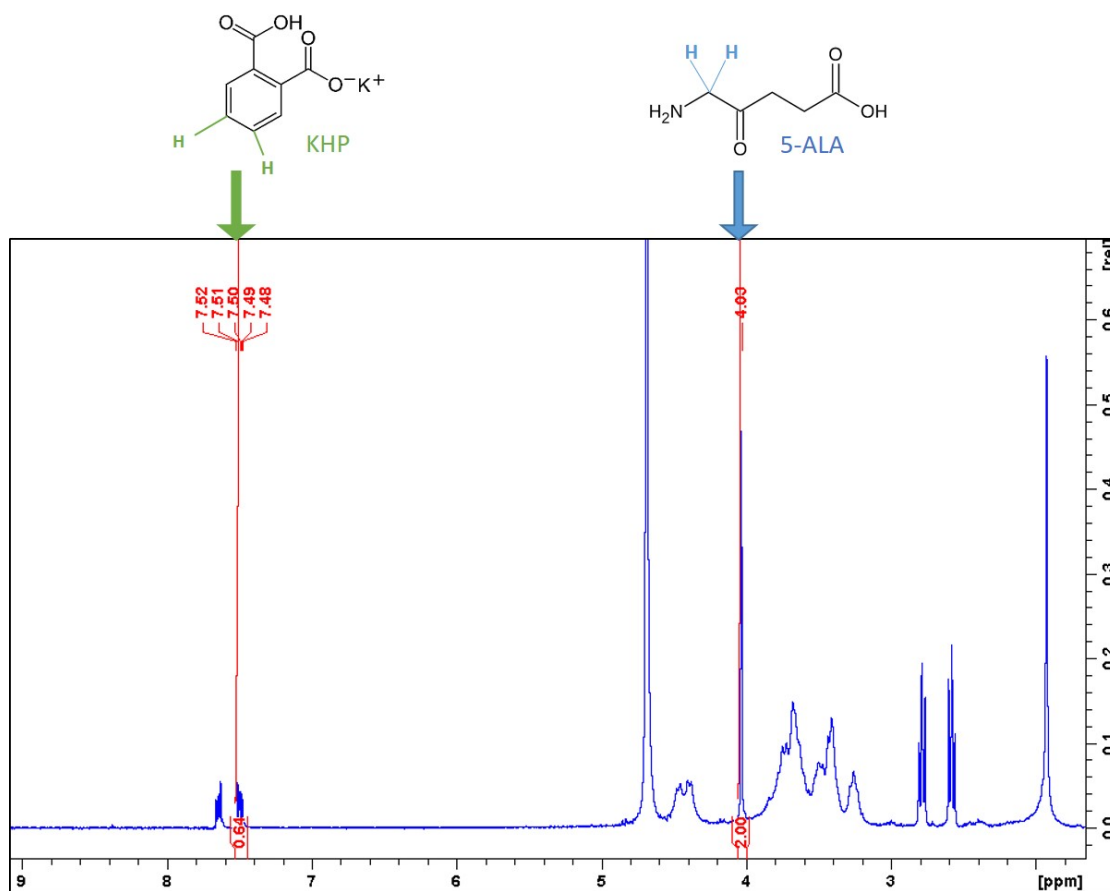


Figure 2:  $^1\text{H}$  NMR spectrum of a piece of MN-20. The integration value of the singlet of 5-ALA at 4.04 ppm was for 2 protons and the integration value of the multiplet of KHP between 7.4 and 7.5 ppm was for 0.64 protons. The others peaks between 2 and 6 ppm are characteristics either of 5-ALA or HA.

viscosity measured at 0.05 Pa s (shear rate:  $50\text{ s}^{-1}$ ).

### 3.2. 5-ALA stability in the MN-patch

255 To ensure a long drug stability, special care was taken by controlling the temperature, the pH and the 5-ALA concentration because these three parameters are considered to be the most influencing for respecting 5-ALA stability [5]. Indeed, 5-ALA is known to be unstable and dimerize in PY, constituting the major degradation product. This is usually a problematic aspect in the design of drug delivery systems intended for photodynamic therapy [30].

260 According to previous studies led by De Blois et al., the risk of 5-ALA to dimerize is reduced when the temperature is decreased to  $21\text{ }^\circ\text{C}$  [31]. The authors modelled the degradation rate of 5-ALA as a second order reaction kinetics and an Arrhenius plot allowed to determine the half

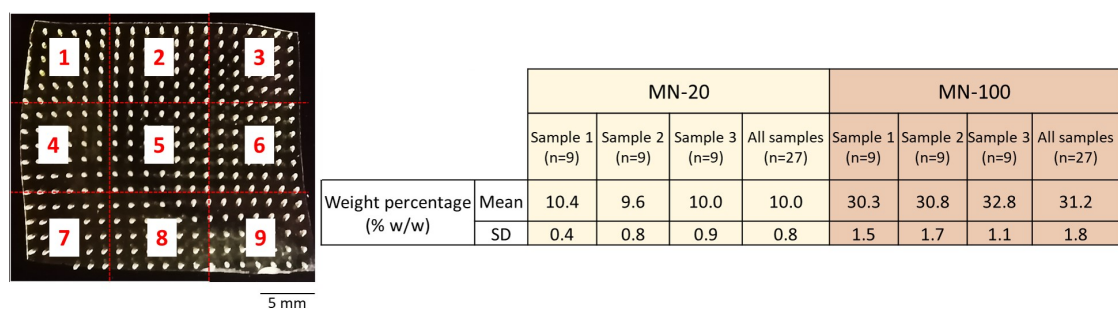


Figure 3: A: photograph of the  $MN_t$ -20 patch, the dotted lines represent the different parts of the patch to evaluate the percentage of 5-ALA in each samples numeroted from 1 to 9. B: table summarizing the weight percentages of 5-ALA in the MN-20 and MN-100 patches. Experiments were repeated three times. Results are presented as mean value  $\pm$  standard deviation.

time<sup>1</sup> of 5-ALA at different temperatures for a solution at  $7.6 \times 10^{-3} \text{ mol L}^{-1}$  and pH 5. At the beginning of the solvent casting molding process, 5-ALA is contained in a polymeric solution and poured in the PDMS mold. At the initial 5-ALA concentration of  $7.6 \times 10^{-2} \text{ mol L}^{-1}$  for MN-20 and  $0.38 \text{ mol L}^{-1}$  for MN-100, by extending the De Blois et al. model, the half times were estimated at 40 days and 8 days for MN-20 and MN-100. During the drying process, for example after 85% of water evaporation, the concentrations will be more elevated and were estimated for MN-20 and MN-100 at  $0.51 \text{ mol L}^{-1}$  and  $2.55 \text{ mol L}^{-1}$  which lead to predicted half lives respectively equal to 6 days and 28 hours. Since the drying step was set at  $40^\circ \text{C}$  for 24 hours, 5-ALA should stay stable in MN-20 but a slight degradation might occur in MN-100.

The second parameter that has been adjusted in order to optimize 5-ALA bioavailability, was the pH, as it is known that 5-ALA is degraded at pH higher than 5 [32]. Since human skin pH is estimated on average at 5 [33], pH 5 has been defined as the optimal value for 5-ALA MN-patch preparation that should not induce skin disorders or irritation when the MN-patch will dissolve [34]. This pH value was adjusted by addition of HCl, with a final concentration of  $3 \text{ mmol L}^{-1}$ .

The third parameter to adjust is the 5-ALA concentration that is required to be kept as low as possible to ensure its stability [35]. Nevertheless, due to the final application in PDT requiring high doses of drug <sup>2</sup>, two high contents of 5-ALA in MN-patches were evaluated (20 mg to 100 mg per patch).

First, the presence of 5-ALA in the MN-patch prepared with a pH solution at 5 and a drying

<sup>1</sup>Half-life can be defined as the time where the 5-ALA concentration reduced to half of its original value.

<sup>2</sup>The conventional PDT treatment using the prodrug in a Metvixia® cream advise to administrate  $\approx 80 \text{ mg}$ .

temperature of 40 °C was confirmed by FTIR. Figure 4 shows the IR spectra of MN-20 and MN-100 compared with those of HA and 5-ALA alone. On the four spectra, the bands observed between 3200-3600, 2850-3000 and 1550-1650  $\text{cm}^{-1}$  were assigned to vibration of OH,  $\text{CH}_2$  and primary  $\text{NH}_2$  respectively. The bands at 1730  $\text{cm}^{-1}$  and at 1600  $\text{cm}^{-1}$  correspond respectively to the carbonyl groups of 5-ALA and the amid group of HA [36, 37]. These two bands appear in MN-20 spectra and are more intense in the MN-100 sample which evidenced the presence of the two compounds in the final material. The band relative to primary amino group is also present in the MN-20 and MN-100 spectra, which confirms the presence of 5-ALA in the patch. MN-20 and MN-100 spectra do not present new large peaks which might suggest that there is no covalent bonds between 5-ALA and HA. Nevertheless, this spectra cannot show that no chemical reaction occurred between the HA polymer and the 5-ALA prodrug. Even if unexpected, since the MN-patch preparation was performed at low temperature (40 °C) without the presence of a coupling agent [38], a reaction between the HA carboxyl group might occur with the amino group present on the 5-ALA to form an amido compound. Infrared spectroscopy correlation table indicates that the characteristic absorption peaks of the amido-group are between 3050-3500  $\text{cm}^{-1}$  (2 large bands), 1630-1710  $\text{cm}^{-1}$  for respectively the vibration of N-H and C=O. Therefore these bands are potentially covered by the HA signal and results of figure 4 cannot strictly confirm that no covalent groups were created.

To further verify that HA was not modified because of 5-ALA,  $^{13}\text{C}$  NMR was performed. As presented in figure 5, all the characteristic peaks of HA were present in the HA that has been in contact with 5-ALA and correspond to the one reported in literature [39, 40]. Some slight shifts (inferior to 1 ppm) may be observed but they have been previously described as conformational rearrangements due to hydrogen bonds [41, 42]. Except at 28 ppm where a low intensity peak was observed due to an impurity, no other peaks were detectable. Consequently, this experiment demonstrate that no covalent bonding was created between 5-ALA and HA. Furthermore the filtrate of the MN-patch isolated with 10 kDa Amicon® Ultra Centrifugal Filters was analysed by  $^1\text{H}$  NMR and only evidenced the presence of 5-ALA with a spectrum similar to pure 5-ALA.

Once no interaction between 5-ALA and HA was proven, the 5-ALA stability was studied. Initially, 5-ALA and PY were separately dissolved in  $\text{D}_2\text{O}$  and figure 6 summarizes the data derived from their  $^1\text{H}$  NMR analysis. The chemical shifts presented were close to those reported in the literature [30, 32, 43]. PY spectrum shows a singlet signal for the aromatic proton (a) at 8.4 ppm and two triplet signals at 3.1 and 2.8 ppm characterising  $\text{CH}_2$  groups (b and c) from the propionic acid chains. 5-ALA spectrum shows a singlet signal for the  $\text{CH}_2$  (x) groups at 4.1

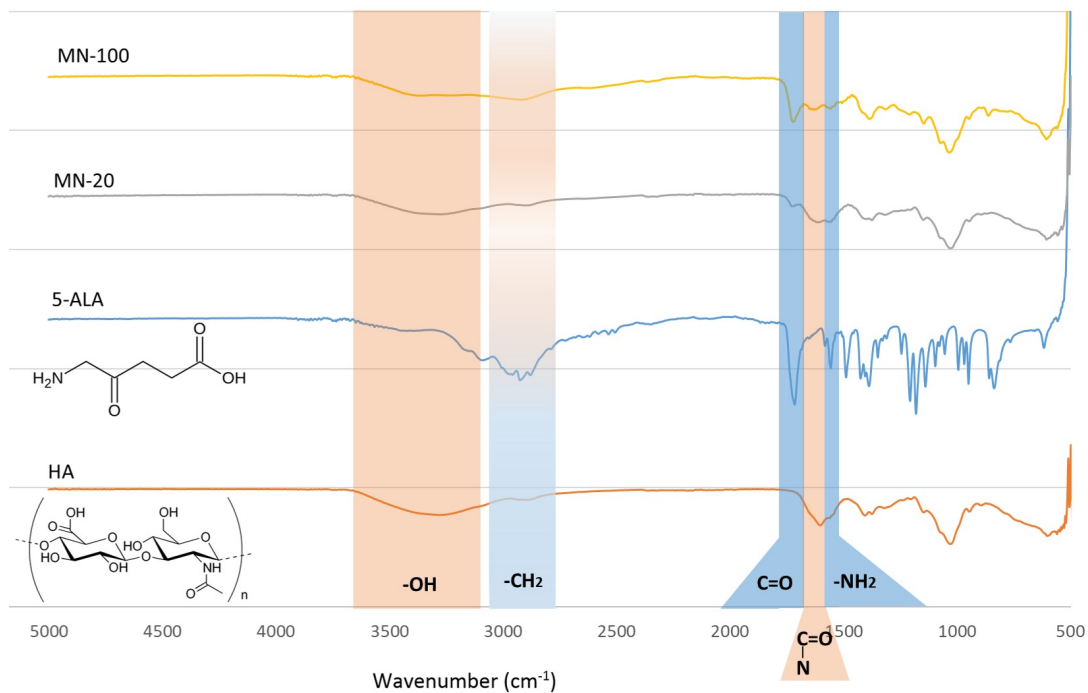


Figure 4: IR spectra of 5-ALA, HA and the microneedle patches MN-20 and MN-100. Blue strips correspond to 5-ALA signature bands and orange strips to HA signature bands.

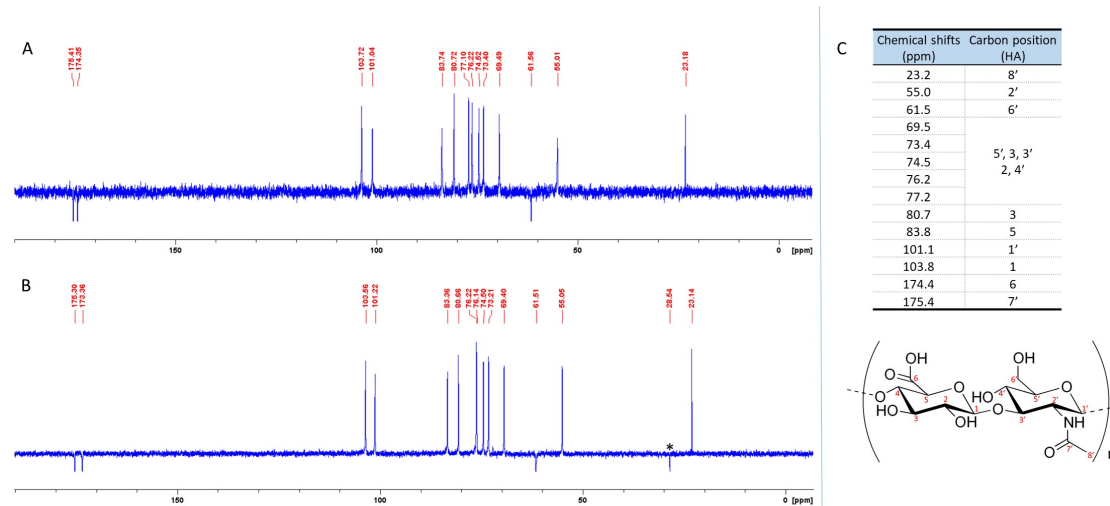
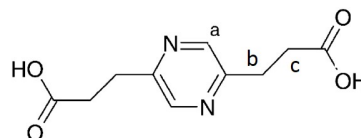


Figure 5: A:  $^{13}\text{C}$  NMR spectrum of MN-0 (HA only). B: HA from MN-20 was isolated with 10kDa Amicon® Ultra Centrifugal Filters, analyzed by  $^{13}\text{C}$  NMR and compared to the one above. C /  $\text{CH}_2$  are down and  $\text{CH} / \text{CH}_3$  are up on the spectrum. C: Structure of HA and summary of the  $^{13}\text{C}$  chemical shifts (parts per million).

315 ppm and two other triplet signals at 2.8 and 2.6 ppm characterizing CH<sub>2</sub> groups (y and z) from the carboxylic acid chain. When 5-ALA and PY are mixed together and analyzed by <sup>1</sup>H NMR the PY triplet signals (b and c) and the 5-ALA triplet signals (y and z) overlap. Only the two singlet signals for the aromatic protons (a) at 8.4 ppm and for the CH<sub>2</sub> (x) groups at 4.1 ppm were still well defined and will be used to quantify the weight percentage of 5-ALA and PY (see 320 equations 1, 2 and 3). No other peaks appears when HA and 5-ALA were mixed together.

Carbon position (PY)	Chemical shifts (ppm)	Multiplet
a	8.4	Single
b	3.1	Triplet
c	2.8	Triplet



Carbon position (5-ALA)	Chemical shifts (ppm)	Multiplet
x	4.1	Single
y	2.8	Triplet
z	2.6	Triplet

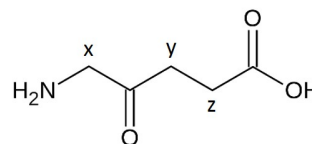


Figure 6: Structure of 2,5-pyrazinedipropionic acid and 5-aminolevulinic acid and summary of <sup>1</sup>H chemical shifts (parts per million)

Figure 7 displays the stability of 5-ALA in the MN-20 patch when stored in hermetic box, containing a desiccant bag, without air at 20 °C and sheltered from light. The weight percentage of 5-ALA evolved from about 10%(w/w) to 7%(w/w) in 145 days. This evolution seems not significant and may be partially due to a slight increase in water content in the MN-20 patch. 325 Indeed TGA experiments showed that the water content was 15%(w/w) after 145 days whereas it was 14%(w/w) at day 1. The adsorption of H<sub>2</sub>O molecules on the microneedles patch may increase the global mass of the patch ( $m_{tot}$ ) and could affect the absolute weight percentage of 5-ALA according to equation 2 which could explain a 1% slight decrease. Overall, this mean value of 7%(w/w) stays in a satisfactory experimental range and evidences a very good stability 330 of 5-ALA in the MN-20 patch over 5 months.

On the other hand, there was no degradation of 5-ALA in PY higher than 1%(w/w) until the 145<sup>th</sup> day. A very limited degradation below 1% during this period is considered as a very encouraging result. Further optimization of storing conditions could be undertaken in order to decrease this degradation level. Indeed, PY is a compound with unknown toxicity and scant 335 information concerning its effect during PDT is available. Its presence should then be kept to

a minimum [44] by avoiding 5-ALA degradation, which should guarantee a safe and successful PDT treatment [30].

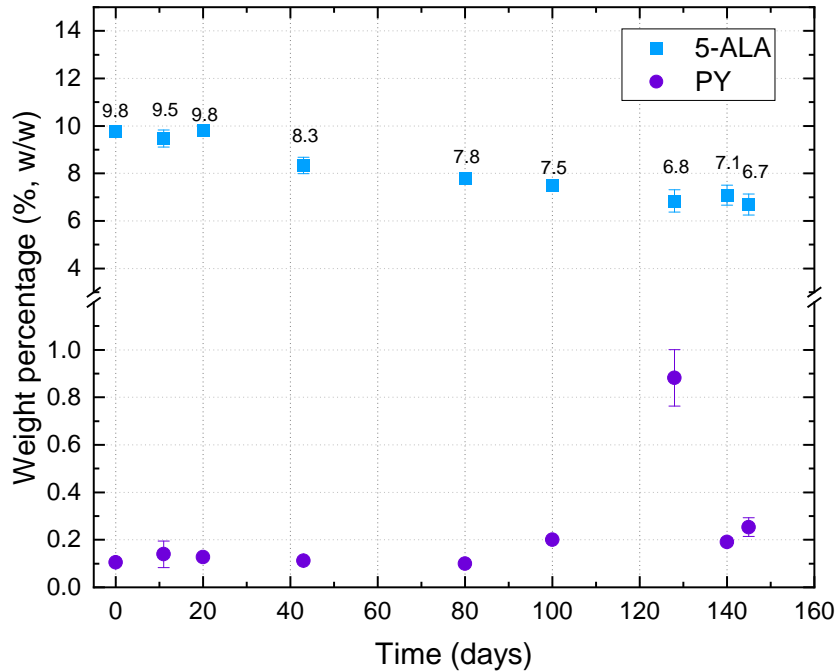


Figure 7: Stability of 5-ALA in the MN-20 patch. Analyses were performed in triplicate. Results are presented as mean value  $\pm$  standard deviation.

Although, all the parameters responsible of 5-ALA stability were not optimized as much as possible, the stability results (figure 7) were satisfactory since they were higher than those expected regarding previous results reported in the literature [30–32].

### 3.3. MN-patch mechanical properties: compression and insertion

#### 3.3.1. Morphology and compression mechanical properties

Prior to biological validations by inserting the patch in skin models or animals skin, it was necessary to control whether the MN-patch had sufficient mechanical properties to pierce the *stratum corneum* without microneedles fracture, bending or height reduction.

Mechanical compression tests were performed to evaluate the MN-patch mechanical strength and results for the  $MN_I$  are displayed in figure 8. There was no significant deformation or fracture

when the compression force applied was below 0.5 N/needle. The loading at 20 or 100 mg in the  $MN_l$ -patch did not affect the mechanical behaviour. A slight height reduction (about 50  $\mu\text{m}$ ) could be observed for the  $MN_l-0$ ,  $MN_l-20$  or  $MN_l-100$  when the force compression applied was equal to 0.5 N/needle. It represents a loss in height of 12.5 %. Almost the same behaviour was observed for the  $MN_t-0$  and  $MN_t-20$  (*results not shown*) since the loss in height do not exceed 7 % even at 0.5 N/needle. For the  $MN_t-100$  at 0.3N/needle and 0.5 N/needle, the loss in height were higher and reached 17 % and 53 %. Nevertheless, the insertion force in the skin was measured with the texturometer and estimated at 0.17 N/needle which insure that insertion could occur without microneedle bending or breaking. The performances of all our needles except  $MN_t-100$  were comparable or even better than the previous reported one indicating a height reduction of ALA-loaded HA microneedle patch (initial height: 900  $\mu\text{m}$ ) of almost 200  $\mu\text{m}$  for a compression force applied of 0.5 N/needle, which corresponds to a loss in height of 22 % [28]. Furthermore, the important height reduction observed for the  $MN_t-100$  might be explained by Zhu et al. work, indicating that the decrease of polymer interactions is due to 5-ALA small molecules that insert between the polymer chains. Consequently, the Young's modulus is decreased and the microneedle become more deformable [29].

In order to gather all required properties for the intended application, the shape of microneedle has been designed in order to reach sufficient mechanical strength for skin insertion, and optimal height for therapeutic indication. To this end, the morphology of the MN-patch developed here consists in a "pencil-tip" shape (Figure 1) that presents an aspect ratio for the  $MN_t$  and  $MN_l$  respectively equal to 5:2 and 4:3 that should be sufficient to pierce and facilitate insertion in the skin [20, 45]. Indeed, the aspect ratio recommended for clinical use by Gittard et al. was 2:1 as it exhibits high mechanical strength and no difficulty for penetration. Nevertheless, this value is only an arbitrary recommendation since they also showed that other aspect ratio such as 3:1 could be efficient too. The most important conclusion of their study showed that when the aspect ratio increased it was associated with lower failure force [45]. Secondly and still to ensure efficient mechanical properties, the base was cylindrical with a diameter fixed at 300  $\mu\text{m}$ . It has been demonstrated that contrary to square or rectangular MN, circular MN can withstand higher forces (stress and bending force) [46]. Thirdly, for the intended application of skin cancer, it is necessary to reach the lower epidermis or the upper dermis without inducing pain or high tissue damages. Thus, depending on the state of the lesions, a low microneedle height of 400  $\mu\text{m}$  or a high one of 750  $\mu\text{m}$  would be the most appropriate. Moreover, these chosen heights are inferior to 900  $\mu\text{m}$  which has been identified as a high value inducing breaking of the

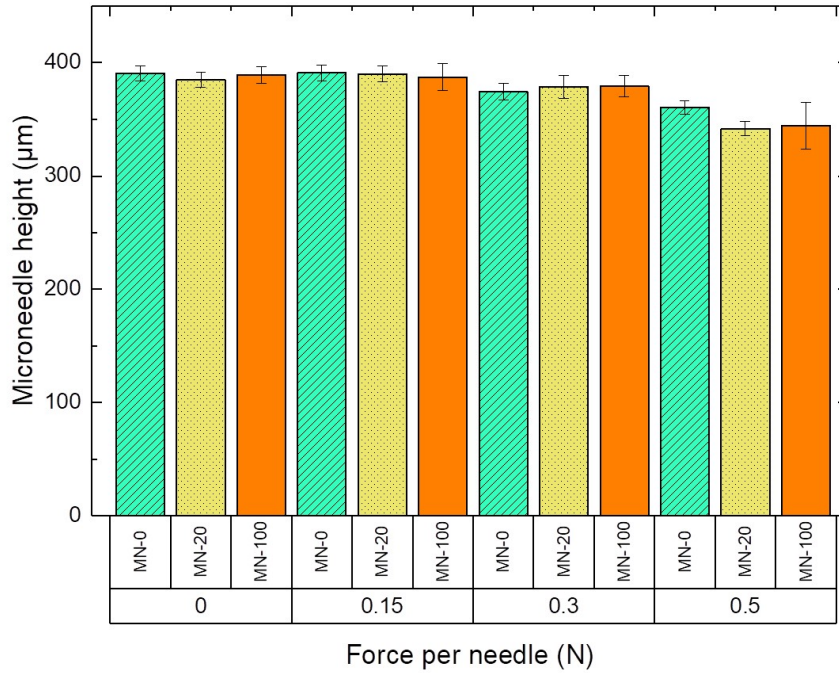


Figure 8: Mechanical behaviour of  $MN_i$  after compression at different forces. Analyses were performed on three different patches with at least 10 height measurements on different microneedles from each patch. Results are presented as mean value  $\pm$  standard deviation.

MNs [46, 47].

### 3.3.2. Insertion tests in *ex vivo* skin and a skin model

Since mechanical strength of microneedles was measured as high enough compared to theoretical skin hardness, it was necessary to further examine their insertion ability. The MN-patch was applied to hair shaved *ex vivo* rat skin and removed. Subsequently, microholes were created on top of the skin and a penetration profile might be observed in cross section. Nevertheless, figure 9 shows that the insertion depth in *ex vivo* rat skin was quite low (less than 20  $\mu\text{m}$ ) which was far shorter than the microneedles height (750  $\mu\text{m}$ ). The main reason of this observation is due to the tissue embedding process with freezing medium which can deeply modify cutaneous

structures by shrinking.

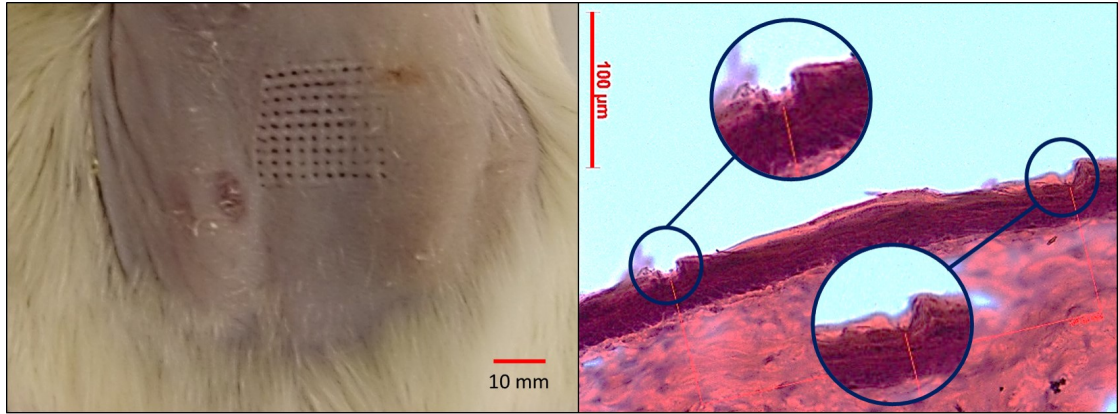


Figure 9: Left: top view observation of rat skin after MN-patch removal. Right: cross section of cryoconserved rat skin after hematoxylin/eosin coloration. The blue circles show the penetration profile of microneedle in the skin.

It was thus necessary to find a skin phantom model with similar mechanical properties and easy to cut without a prior embedding process in order to assess the puncture ability of our device. Classically, gelatin based gels are used but as it is prepared in water, HA-based MN dissolved very rapidly during insertion assay. In order to overcome this difficulty, a Plastiline® material made of oils, mineral waxes and fillers has been chosen with a Young's modulus measured at 10 kPa very close from the skin's one. Therefore it was possible to observe the microchannels created after insertion.

After microneedles insertion, a slice of the skin phantom was manually cut under a binocular magnifier with a scalpel following a ruler. The cross-section observation suggests that the insertion depth was about  $374 \pm 10 \mu\text{m}$  and  $594 \pm 61 \mu\text{m}$  for respectively  $MN_l$  and  $MN_t$  as presented in figure 10. Larrañeta et al. worked on another alternative that consists in assembling multiple layers of Parafilm™. Authors then inserted the microneedles and evaluated the percentage of holes created in each Parafilm™ layer [48]. As Plastiline®, Parafilm™ method allows to develop a rapid microneedle quality control. Similarly, Enfield et al. chose a Blu-Tack® material which is a pressure-sensitive clay-like adhesive known for its low elasticity and soft pliable consistency [49]. The microneedle array with a needle height of  $280 \mu\text{m}$  was inserted into this artificial material and the micropores created were observed under optical coherence tomography system. The depth penetration measured on Blu-Tack® material and forearm skin were respectively  $254 \pm 7 \mu\text{m}$  and  $179 \pm 14 \mu\text{m}$  [49]. Overall, materials mimicking tissue (Plastiline®, Parafilm™ or Blu-Tack®)

appeared to be good alternatives to biological tissue for MN insertion studies however the depth penetration might be overvalued as shown by Enfield et al. [49].

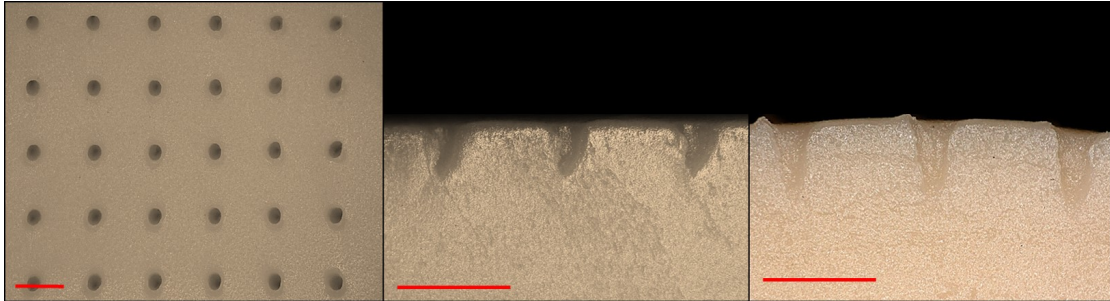


Figure 10: Left: top view observation of phantom skin after MN-patch removal. Middle: cross section of phantom skin after  $MN_i$  removal. Right: cross section of phantom skin after  $MN_t$  removal. Experiments repeated 5 times. Scale bars represent  $1000\ \mu\text{m}$ .

On the other hand, top view observation on *ex vivo* rat skin (figure 9, left) and on the membrane model (figure 10, left) evidenced that microneedles had perforated the skin barrier since  
 415 microholes were observed. The interval between them was equal to  $1200\ \mu\text{m}$  which corresponds well to the original spacing on master structure. Pore diameters created were measured on the Plastiline membrane model at  $269 \pm 10\ \mu\text{m}$  which is close to the microneedle base diameter set up at  $300\ \mu\text{m}$ .

In addition, the spacing between the microneedles has been demonstrated as a parameter  
 420 influencing the insertion force required to make the microneedles penetrate through the skin. Indeed, Olatunji et al. developed Gantrez<sup>®</sup> microneedles and showed that the insertion forces required for  $330\ \mu\text{m}$  tip-spaced MNs (16 MNs/array) and  $900\ \mu\text{m}$  tip-spaced MNs (4 MNs/array) were respectively equal to  $0.030\ \text{N/needle}$  and  $0.028\ \text{N/needle}$  (insertion speed of  $0.5\ \text{N mm}^{-1}$ ) [50]. Another study led by Kochhar et al. established that penetration percentage was more  
 425 important when spacing between MNs tips increased. For instance, they revealed that microneedles (microneedle array:  $1.44\ \text{cm}^2$ ) with a base diameter set at  $300\ \mu\text{m}$  and a tip-interspacing of  $1800\ \mu\text{m}$  had optimal characteristics to penetrate the skin with 64% penetration [51]. A large spacing also avoids to form a “bed of nails” described by the same authors as a too high density of microneedles that reduce penetration and efficiency of microneedle penetration [51]. Moreover  
 430 a high density of microneedles is also restrictive as demonstrated by Gill et al. who showed that a 10-fold increase in the number of microneedles is two-fold more painful [12]. In this study, in agreement with these previous research works, the spacing between microneedle tips was set

at 1200  $\mu\text{m}$  with 400 MNs/array. Such parameters enable easy manual MN-patch insertion as presented in figures 9 and 10, would be sufficient for high dose delivery while avoiding crowding, and should ensure a minimal pain.

#### 3.4. Dissolution rate of the MN-patch after insertion in *ex vivo* rat skin, release kinetics of 5-ALA and MN-patch biocompatibility

HA has been widely used the last decade as a component of artificial matrices and in bio-engineering for tissue scaffolding or skin reparation. HA is known to be a highly water-soluble polysaccharide. Consequently when the HA-based MN-patch will be applied on the skin, which is approximately composed of 70 % of water, it is firstly expected that the MN-patch dissolves and releases 5-ALA [52]. When the whole patch will be dissolved into the skin, HA will be further biodegraded since this polymer is already present in the human body and naturally degraded. In fact, the catabolism of HA has been widely described in the literature as a depolymerization process due to the enzymatic cleavage of glycosidic linkages leading to smaller molecule chains. These smaller molecules are naturally present in the human body and will join the natural elimination process consisting in a degradation metabolism in liver or lymph nodes thanks to endothelial cells. The half-life of HA was estimated between 1 and several days. Then the remainder enters in the bloodstream and is eliminated with a half-life between 2 and 5 min [53–55]. Therefore, HA is a good candidate to be dissolved by the skin, leading to 5-ALA release, and be furthermore rapidly biodegraded by a natural enzymatic pathway.

Kinetics of MN-patch dissolution was estimated by removing the patch from the *ex vivo* skin at different times and results are displayed in figure 11. At 10 min, there was no obvious dissolution for the  $MN_l$  whereas  $MN_t$  dissolution was initiated. This fact could be explained by the  $MN_t$  size that can reach deeper skin layer and particularly the lower dermis which is more hydrated and could enhance HA dissolution. A significant dissolution for both patches ( $MN_l$  or  $MN_t$ ) occurred after 45 min. After 60 min, the disintegration of the patch base was noticeable. These experiments showed that when the MN-patch will be applied on the skin, a first drug release at 45 minutes time scale will take place due to microscale needles fast dissolution. Then a second slower drug release at 60 minutes time scale will occur due to the MN-patch base disintegration and could constitute a drug reservoir.

However, the dissolution was not homogenous. Indeed, MN-patch surface is quite large ( $25 \times 25 \text{ mm}^2$ ) and it is conceivable that the entire patch do not receive homogenous force which lead to partial microneedle penetration and inhomogenous dissolution. Different studies have

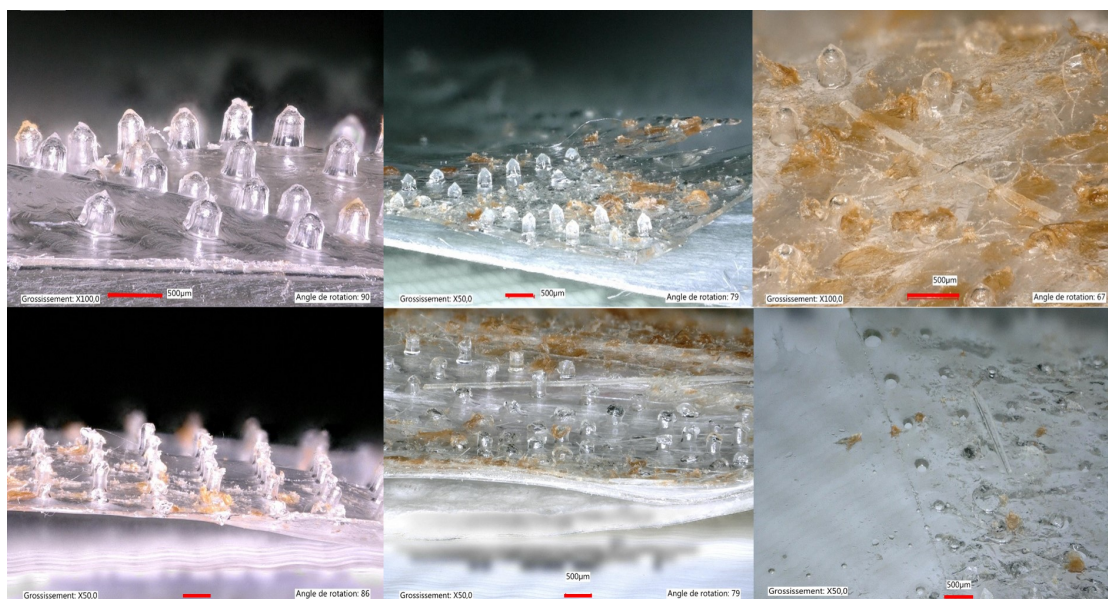


Figure 11: Microscopic images of microneedle patches after their application to *ex vivo* rat skin. Upper line corresponds to  $MN_l$  and lower line to  $MN_t$ . From left to right: 10, 45 and 60 min. Scale bars represent 500  $\mu\text{m}$ .

465 been conducted to developed microneedle applicator, nevertheless they are rigid and are not  
suitable to be applied on body curves[56]. Ripolin et al. conducted a study where they hold  
a pressure for 45s and then use a strong adhesive to fix the microneedle patch into the skin.  
They proved a successful insertion but there was no microscopical images of the microneedle  
disintegration [57]. Overall, adhesive bandages may be an effective solution to ensure microneedle  
470 insertions and keeping them into the skin. Nevertheless, if the lesion is located on the nose a  
bandage may be unsuitable to maintain a pressure on the MN-patch and a thumb pressure may  
be more easier to perform. Therefore, the force that 8 people exerted spontaneously with their  
thumb, for 10 seconds using the texturometer was measured. We have observed that when the  
indication was “apply a pressure on the whole patch that could allow its insertion in the skin”  
475 the force was measured at  $24.5 \pm 7.5 \text{ N}$  which represent 0.34 N/needle and is higher than the one  
needed for good needles insertion in the skin.

In the other hand, the dissolution rate can be controllable by the initial polymer solution  
i.e HA concentration and/or HA molecular mass. Indeed, a lower HA concentration will result  
in a faster dissolution. Similarly an upper HA molecular mass will lead to a lower dissolution  
480 due to stronger entanglement between polymeric chains (*Preliminary experiments were realized  
on gelatin phantom skin and are not presented here*). In fact, Leone et al. have also described

these properties and they mentioned that a balance may be found between dissolution rate and mechanical properties since a lower molecular (4.9 kDa) mass may dissolve faster than upper one at 4.9 kDa but microneedles appeared less robust [58].

485 This first evaluation of MN-patch dissolution rate was comforting with the end-use application desired. Nevertheless, on *ex vivo* rat skin, it was not possible to evaluate the amount of 5-ALA released at predetermined time points because a long extraction protocol would have been necessary and might have degraded the 5-ALA. Therefore, an *in vitro* drug release experiment was set up in an attempt to mimic the dissolution rate observed in *ex vivo* rat skin. Indeed, after  
490 80 min, macroscopic observation highlighted that the patch was almost completely dissolved as it was after 60 min in *ex vivo* rat skin. As displayed in figure 12, the amount of 5-ALA released was respectively equal to 77% and 88% for MN-20 and MN-100. Therefore, it may be assumed that these quantities may also be released during *ex vivo* or *in vivo* experiments which could be a sufficient quantity to perform a PDT treatment in a reasonable time-frame.  
495 The 5-ALA release kinetics of MN-100 appears to be slightly faster than that of the MN-20 patch. Indeed, drug delivery is governed by diffusion through the polymer (Fick's law) and by the polymer dissolution (due to convection) [59]. Considering that MN-100 contains more 5-ALA, the prodrug diffusion through the microneedles might be more intense and explain this larger 5-ALA percentage released. Overall, the ability of the patch to deliver 5-ALA in a short  
500 time period ( $< 1h30$ ) is impressive compared to previous studies [60–62]. For example in 2006, McCarron et al. showed that a bioadhesive patch made of poly(methyl vinyl ether-co-maleic anhydride) and tripropyleneglycol methyl ether and containing either  $19 \text{ mg cm}^{-2}$  or  $50 \text{ mg cm}^{-2}$  of 5-ALA only released 57% in 6 hours [63]. However, the *in vitro* measurements that the authors investigated were conducted with a Franz diffusion cell and they only dosed the amount that  
505 cross all the skin phantom. We may assume that 5-ALA was still contained in the skin itself. Although 5-ALA is a key parameter at the origin of PpIX production, instead of dosing this prodrug precursor, it would also be interesting to evaluate the amount of PpIX itself by testing the patches *in vivo* on skin lesions in order to evaluate PpIX accumulation in the different skin layers [61].

510 Since dissolution was effective on *ex vivo* rat skin, and release of 5-ALA was effective, it is now important to control its cytotoxicity with a view to future use of this device *in vivo*. To evaluate the biocompatibility of the MN-20 and MN-100 patches, a WST-1 cytotoxicity assay was performed and results are presented in figure 13.

The density of living cells cultured in medium which were in contact with MN-0 was com-

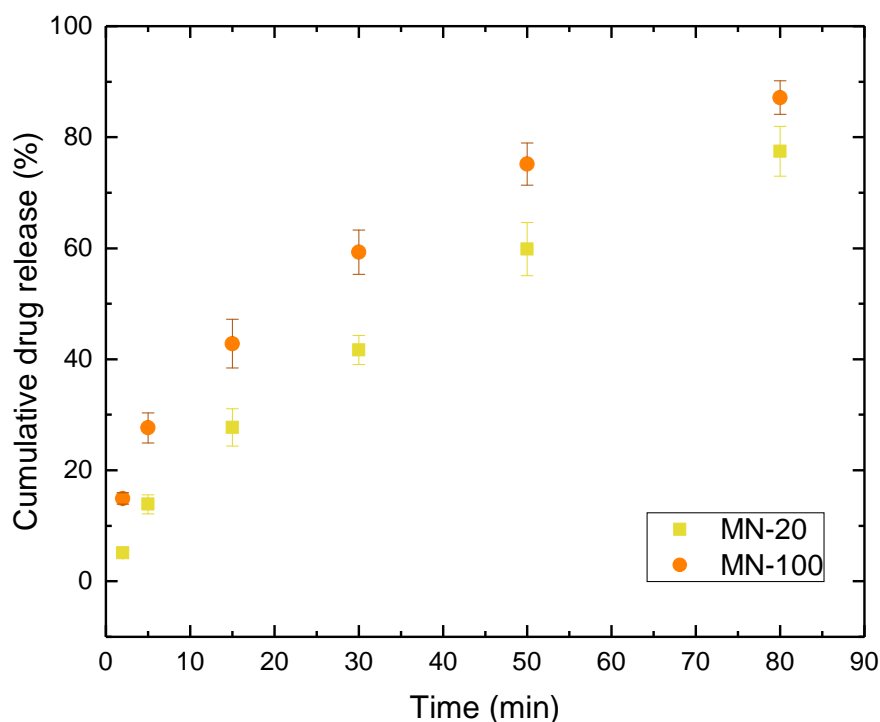


Figure 12: Cumulative amount of released 5-ALA in water at  $pH5$  from MN-20 and MN-100 patches during 80 min.

515 parable to the negative control indicating that MN-0 was not cytotoxic. It was expected since MN-0 was only composed of HA and this polymer is well known for its biocompatibility as a naturally occurring biopolymer. For example, in a 70 kg-human body roughly 15 g of HA is present and 50 % is concentrated in the skin [64]. Developing HA based microneedles was relevant and cytotoxicity experiments approved it.

520 Furthermore the density of the living cells cultured in medium which were in contact with MN-20 and MN-100 were also comparable to the negative control no matter the concentration. As the MN-p contained 5-ALA and PY, different conditions with these two molecules were also tested and results are displayed in figure 14. As presented in section 3.1, the weight percentages of 5-ALA in the MN-20 and MN-100 were respectively equal to 10.0%(w/w) and 525 31.2%(w/w). Therefore, when the cytotoxicity of the patch was tested at the higher concentration ( $40 \mu\text{g mL}^{-1}$ ), the 5-ALA concentration was at most equal to  $4.0 \mu\text{g mL}^{-1}$  or  $12.5 \mu\text{g mL}^{-1}$

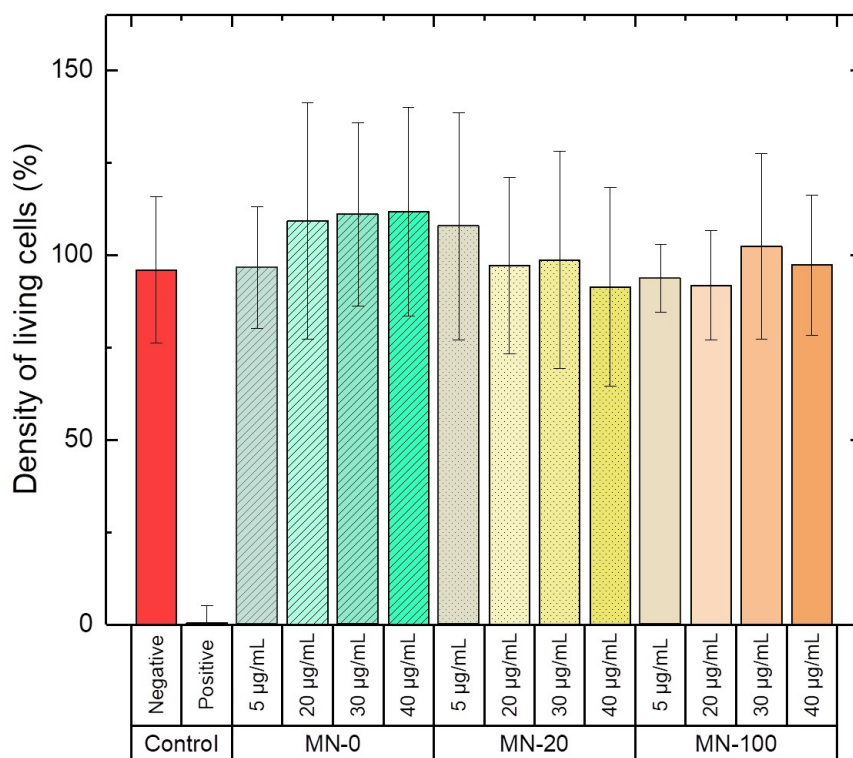


Figure 13: Density of living NIH3T3 fibroblasts after 24 h incubation with MN-0, MN-20, or MN-100. Negative control corresponds to cells incubated in medium only. Positive control corresponds to cells incubated in medium containing  $H_2O_2$ .

and these concentrations appeared to be non cytotoxic for the cells (figure 14, left) which was comparable to the results obtained in the litterature by Li et al., Dan et al. [65, 66]. Moreover, the density of living cells after contact with PY remains about 100% which was comfoting as a

530 1% degradation of 5-ALA in PY was observed in MN-patch.

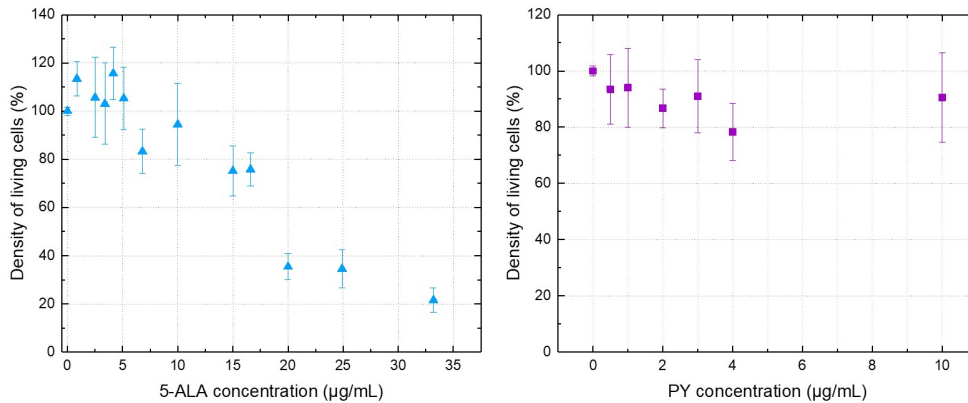


Figure 14: Density of living NIH3T3 fibroblasts after 24 h incubation with 5-ALA or PY.

#### 4. Conclusion

Microneedle patches were fabricated by a single step of solvent casting molding method. The manufacture way very easy, low cost and relevant which would allow a facile translation of this technology. Two heights were developed: 400 µm and 750 µm. Each microneedle patch could contain 20 mg or 100 mg of 5-ALA consequently a single application is sufficient to deliver the amount required for PDT treatment. 5-ALA stability was followed to ensure that there was no dimerization in PY and exhibited a very good stability in the MN-patch even 5 months after manufacturing. Mechanical compression tests were performed and the different kinds of MN-patches do not present a significant deformation when the force applied was not superior to 0.3 N/needle. These results suggested that MN-patch had efficient strength to pierce the *stratum corneum*. Indeed, *ex vivo* rat skin was well perforated due to microneedle application since micropores were created. A clear penetration profile was distinguishable on phantom skin with depth penetration of  $374 \pm 10$  µm and  $594 \pm 61$  µm for respectively  $MN_l$  and  $MN_t$ . Dissolution rate was estimated on *ex vivo* rat skin demonstrating that the microneedles were dissolved within 45 min and the support started to dissolve after 60 min.

According to the previous results, MN-patches might be a promising technique to enhance 5-ALA penetration and produce PpIX in deeper skin lesions. In the very near future, *in vivo* tests on rats suffering from precancerous skin lesions will be carried out to show microneedle possible benefit during PDT treatment.

## 550 Acknowledgments

This project is supported by the European Union – European Regional Development Fund. LETI/DTBS is supported by the French National Research Agency in the framework of the “Investissement d'avenir” program Glyco@Alps (ANR-15-IDEX-02) and Arcane Labex (ANR-12-LABX-003). The authors would also like to thank Manuel Alessio for the design of the  
555 aluminium microneedle master structure. Mathilde Menneteau is also acknowledged for her help with cytotoxicity experiments. The authors are grateful to Nicolas Duraffourg for assistance with the NMR analysis.

## References

- [1] J. Escobar-Chavez, R. Diaz-Torres, I. M. Rodriguez-Cruz, Dominguez-Delgado, Sampere-Morales, Angeles-Anguiano, Melgoza-Contreras, Nanocarriers for transdermal drug delivery, Research and Reports in Transdermal Drug Delivery (2012) 3. doi:10.2147/RRTD.S32621.
- [2] S. F. Taveira, R. F. V. Lopez, Topical administration of anticancer drugs for skin cancer treatment, in: Skin Cancers-Risk Factors, Prevention and Therapy, InTech, 2011.
- [3] R. Lutton, J. Moore, E. Larrañeta, S. Ligett, R. F. Donnelly, Microneedle characterisation: The need for universal acceptance criteria and GMP specifications when moving towards commercialisation, Drug Delivery and Translational Research 5 (2015) 313–331. doi:10.1007/s13346-015-0237-z.
- [4] M.-C. Kearney, S. Brown, M. T. McCrudden, A. J. Brady, R. F. Donnelly, Potential of microneedles in enhancing delivery of photosensitising agents for photodynamic therapy, Photodiagnosis and Photodynamic Therapy 11 (2014) 459–466. doi:10.1016/j.pdpdt.2014.09.003.
- [5] M. Champeau, S. Vignoud, L. Mortier, S. Mordon, Photodynamic therapy for skin cancer: How to enhance drug penetration?, Journal of Photochemistry and Photobiology B: Biology 197 (2019) 111544. doi:10.1016/j.jphotobiol.2019.111544.
- [6] R. F. Donnelly, D. I. J. Morrow, M. T. C. McCrudden, A. Z. Alkilani, E. M. Vicente-Pérez, C. O'Mahony, P. González-Vázquez, P. A. McCarron, A. D. Woolfson, Hydrogel-Forming and Dissolving Microneedles for Enhanced Delivery of Photosensitizers and Precursors, Photochemistry and Photobiology 90 (2014) 641–647. doi:10.1111/php.12209.

- [7] J. Lin, M. T. Wan, Current evidence and applications of photodynamic therapy in dermatology, *Clinical, Cosmetic and Investigational Dermatology* (2014) 145. doi:10.2147/CCID.S35334.
- [8] R. F. Donnelly, D. I. Morrow, P. A. McCarron, A. D. Woolfson, A. Morrissey, P. Juzenas, A. Juzeniene, V. Iani, H. O. McCarthy, J. Moan, Microneedle-mediated intradermal delivery of 5-aminolevulinic acid: Potential for enhanced topical photodynamic therapy, *Journal of Controlled Release* 129 (2008) 154–162. doi:10.1016/j.jconrel.2008.05.002.
- [9] R. F. Donnelly, D. I. Morrow, P. A. McCarron, A. David Woolfson, A. Morrissey, P. Juzenas, A. Juzeniene, V. Iani, H. O. McCarthy, J. Moan, Microneedle arrays permit enhanced intradermal delivery of a preformed photosensitizer, *Photochemistry and photobiology* 85 (2009) 195–204.
- [10] J. W. Lee, K. H. Yoo, B. J. Kim, M. N. Kim, Photodynamic therapy with methyl 5-aminolevulinate acid combined with microneedle treatment in patients with extensive alopecia areata: Correspondence, *Clinical and Experimental Dermatology* 35 (2009) 548–549. doi:10.1111/j.1365-2230.2009.03695.x.
- [11] R. F. Donnelly, D. I. Morrow, T. R. Singh, K. Migalska, P. A. McCarron, C. O’Mahony, A. D. Woolfson, Processing difficulties and instability of carbohydrate microneedle arrays, *Drug Development and Industrial Pharmacy* 35 (2009) 1242–1254. doi:10.1080/03639040902882280.
- [12] H. S. Gill, D. D. Denson, B. A. Burris, M. R. Prausnitz, Effect of Microneedle Design on Pain in Human Volunteers, *The Clinical Journal of Pain* 24 (2008) 585–594. doi:10.1097/AJP.0b013e31816778f9.
- [13] M. R. Prausnitz, R. Langer, Transdermal drug delivery, *Nature Biotechnology* 26 (2008) 1261–1268. doi:10.1038/nbt.1504.
- [14] F. S. Iliescu, D. Dumitrescu-Ionescu, M. Petrescu, C. Iliescu, A review on transdermal drug delivery using microneedles: Current research and perspective, *Ann. Acad. Rom. Sci* 7 (2014) 7–34.
- [15] R. F. Donnelly, D. I. J. Morrow, M. T. C. McCrudden, A. Z. Alkilani, E. M. Vicente-Pérez, C. O’Mahony, P. González-Vázquez, P. A. McCarron, A. D. Woolfson, Hydrogel-Forming

- and Dissolving Microneedles for Enhanced Delivery of Photosensitizers and Precursors, *Photochemistry and Photobiology* 90 (2014) 641–647. doi:10.1111/php.12209.
- 610 [16] S. Liu, M.-n. Jin, Y.-s. Quan, F. Kamiyama, K. Kusamori, H. Katsumi, T. Sakane, A. Yamamoto, Transdermal delivery of relatively high molecular weight drugs using novel self-dissolving microneedle arrays fabricated from hyaluronic acid and their characteristics and safety after application to the skin, *European Journal of Pharmaceutics and Biopharmaceutics* 86 (2014) 267–276. doi:10.1016/j.ejpb.2013.10.001.
- 615 [17] M. Cormier, B. Johnson, M. Ameri, K. Nyam, L. Libiran, D. D. Zhang, P. Daddona, Transdermal delivery of desmopressin using a coated microneedle array patch system, *Journal of Controlled Release* 97 (2004) 503–511. doi:10.1016/j.jconrel.2004.04.003.
- [18] A. K. Jain, C. H. Lee, H. S. Gill, 5-Aminolevulinic acid coated microneedles for photodynamic therapy of skin tumors, *Journal of Controlled Release* 239 (2016) 72–81. doi:10.1016/j.jconrel.2016.08.015.
- 620 [19] T. Miyano, Y. Tobinaga, T. Kanno, Y. Matsuzaki, H. Takeda, M. Wakui, K. Hanada, Sugar micro needles as transdermic drug delivery system, *Biomedical Microdevices* 7 (2005) 185–188.
- [20] J. W. Lee, J.-H. Park, M. R. Prausnitz, Dissolving microneedles for transdermal drug delivery, *Biomaterials* 29 (2008) 2113–2124. doi:10.1016/j.biomaterials.2007.12.048.
- 625 [21] S. P. Sullivan, D. G. Koutsonanos, M. del Pilar Martin, J. W. Lee, V. Zarnitsyn, S.-O. Choi, N. Murthy, R. W. Compans, I. Skountzou, M. R. Prausnitz, Dissolving polymer microneedle patches for influenza vaccination, *Nature Medicine* 16 (2010) 915–920. doi:10.1038/nm.2182.
- 630 [22] J. W. Lee, S.-O. Choi, E. I. Felner, M. R. Prausnitz, Dissolving Microneedle Patch for Transdermal Delivery of Human Growth Hormone, *Small* 7 (2011) 531–539. doi:10.1002/smll.201001091.
- [23] J.-H. Park, M. G. Allen, M. R. Prausnitz, Polymer Microneedles for Controlled-Release Drug Delivery, *Pharmaceutical Research* 23 (2006) 1008–1019. doi:10.1007/s11095-006-0028-9.
- 635 [24] A. Nayak, D. B. Das, Potential of biodegradable microneedles as a transdermal delivery vehicle for lidocaine, *Biotechnology Letters* 35 (2013) 1351–1363. doi:10.1007/s10529-013-1217-3.

- [25] J. Necas, L. Bartosikova, P. Brauner, J. Kolar, Hyaluronic acid (hyaluronan): A review, *Veterinární Medicína* 53 (2008) 397–411. doi:10.17221/1930-VETMED.
- 640 [26] Z. Zhu, H. Luo, W. Lu, H. Luan, Y. Wu, J. Luo, Y. Wang, J. Pi, C. Y. Lim, H. Wang, Rapidly Dissolvable Microneedle Patches for Transdermal Delivery of Exenatide, *Pharmaceutical Research* 31 (2014) 3348–3360. doi:10.1007/s11095-014-1424-1.
- [27] J. Mönkäre, M. Reza Nejadnik, K. Baccouche, S. Romeijn, W. Jiskoot, J. A. Bouwstra, IgG-loaded hyaluronan-based dissolving microneedles for intradermal protein delivery, *Journal of Controlled Release* 218 (2015) 53–62. doi:10.1016/j.jconrel.2015.10.002.
- 645 [28] X. Zhao, X. Li, P. Zhang, J. Du, Y. Wang, Tip-loaded fast-dissolving microneedle patches for photodynamic therapy of subcutaneous tumor, *Journal of Controlled Release* 286 (2018) 201–209. doi:10.1016/j.jconrel.2018.07.038.
- [29] J. Zhu, L. Dong, H. Du, J. Mao, Y. Xie, H. Wang, J. Lan, Y. Lou, Y. Fu, J. Wen, B. Jiang, Y. Li, J. Zhu, J. Tao, 5-Aminolevulinic Acid-Loaded Hyaluronic Acid Dissolving Microneedles for Effective Photodynamic Therapy of Superficial Tumors with Enhanced Long-Term Stability, *Advanced Healthcare Materials* 8 (2019) 1900896. doi:10.1002/adhm.201900896.
- 650 [30] P. A. McCarron, R. F. Donnelly, A. D. Woolfson, G. P. Andrews, Analysis of pyrazine 2,5-dipropionic acid in 5-aminolevulinic acid-loaded urological and topical delivery vehicles: Methodology and assay validation, *Journal of Pharmaceutical and Biomedical Analysis* 36 (2005) 1099–1105. doi:10.1016/j.jpba.2004.09.004.
- 655 [31] A. W. De Blois, R. J. E. Grouls, E. W. Ackerman, W. J. A. Wijdeven, Development of a stable solution of 5-aminolaevulinic acid for intracutaneous injection in photodynamic therapy, *Lasers in medical science* 17 (2002) 208–215.
- [32] A. Bunke, O. Zerbe, H. Schmid, G. Burmeister, H. P. Merkle, B. Gander, Degradation mechanism and stability of 5-aminolevulinic acid, *Journal of pharmaceutical sciences* 89 (2000) 1335–1341.
- 660 [33] H. Lambers, S. Piessens, A. Bloem, H. Pronk, P. Finkel, Natural skin surface pH is on average below 5, which is beneficial for its resident flora, *International Journal of Cosmetic Science* 28 (2006) 359–370. doi:10.1111/j.1467-2494.2006.00344.x.
- 665

- [34] L. Baranda, R. Gonzalez-Amaro, B. Torres-Alvarez, C. Alvarez, V. Ramirez, Correlation between pH and irritant effect of cleansers marketed for dry skin, *International Journal of Dermatology* 41 (2002) 494–499. doi:10.1046/j.1365-4362.2002.01555.x.
- [35] B. Elfsson, I. Wallin, S. Eksborg, K. Rudaeus, A. M. Ros, H. Ehrsson, Stability of 5-aminolevulinic acid in aqueous solution, *European journal of pharmaceutical sciences* 7 (1999) 87–91.
- [36] J. Chen, Q. Peng, H.-J. Jodl, Infrared spectral comparison of 5-aminolevulinic acid and its hexyl ester, *Spectrochimica Acta Part A: Molecular and Biomolecular Spectroscopy* 59 (2003) 2571–2576. doi:10.1016/S1386-1425(03)00011-8.
- [37] K. J. Reddy, K. T. Karunakaran, Purification and characterization of hyaluronic acid produced by *Streptococcus zooepidemicus* strain 3523-7, *Journal of BioScience and Biotechnology* (2013) 7.
- [38] P. Bulpitt, D. Aeschlimann, New strategy for chemical modification of hyaluronic acid: Preparation of functionalized derivatives and their use in the formation of novel biocompatible hydrogels (1998) 18.
- [39] M. A. Napier, N. M. Hadler, Effect of calcium on structure and function of a hyaluronic acid matrix: Carbon-13 nuclear magnetic resonance analysis and the diffusional behavior of small solutes, *Proceedings of the National Academy of Sciences* 75 (1978) 2261–2265. doi:10.1073/pnas.75.5.2261.
- [40] N. Izawa, T. Hanamizu, R. Iizuka, T. Sone, H. Mizukoshi, K. Kimura, K. Chiba, *Streptococcus thermophilus* produces exopolysaccharides including hyaluronic acid, *Journal of Bioscience and Bioengineering* 107 (2009) 119–123. doi:10.1016/j.jbiosc.2008.11.007.
- [41] B. J. Kvam, M. Atzori, R. Toffanin, S. Paoletti, F. Biviano, <sup>1</sup>H- and <sup>13</sup>C-NMR studies of solutions of hyaluronic acid esters and salts in methyl sulfoxide: Comparison of hydrogen-bond patterns and conformational behaviour, *Carbohydrate Research* 230 (1992) 1–13. doi:10.1016/S0008-6215(00)90509-3.
- [42] M. K. Cowman, D. M. Hittner, J. Feder-Davis, C-NMR Studies of Hyaluronan: Conformational Sensitivity to Varied Environments, *Macromolecules* 29 (1996) 2894–2902. doi:10.1021/ma951701x.

- 695 [43] E. K. Jaffe, J. S. Rajagopalan, Nuclear magnetic resonance studies of 5-aminolevulinate demonstrate multiple forms in aqueous solution, *Bioorganic Chemistry* 18 (1990) 381–394. doi:10.1016/0045-2068(90)90022-W.
- [44] R. F. Donnelly, P. A. McCarron, D. A. Woolfson, Derivatives of 5-aminolevulinic acid for photodynamic therapy, *Perspectives in medicinal chemistry* 1 (2007) 1177391X0700100005.
- 700 [45] S. D. Gittard, B. Chen, H. Xu, A. Ovsianikov, B. N. Chichkov, N. A. Monteiro-Riviere, R. J. Narayan, The effects of geometry on skin penetration and failure of polymer microneedles, *Journal of Adhesion Science and Technology* 27 (2013) 227–243. doi:10.1080/01694243.2012.705101.
- [46] P. Aggarwal, C. Johnston, Geometrical effects in mechanical characterizing of microneedle for biomedical applications, *Sensors and Actuators B: Chemical* 102 (2004) 226–234. doi:10.1016/j.snb.2004.04.024.
- 705 [47] S. P. Davis, B. J. Landis, Z. H. Adams, M. G. Allen, M. R. Prausnitz, Insertion of microneedles into skin: Measurement and prediction of insertion force and needle fracture force, *Journal of Biomechanics* 37 (2004) 1155–1163. doi:10.1016/j.jbiomech.2003.12.010.
- 710 [48] E. Larrañeta, J. Moore, E. M. Vicente-Pérez, P. González-Vázquez, R. Lutton, A. D. Woolfson, R. F. Donnelly, A proposed model membrane and test method for microneedle insertion studies, *International Journal of Pharmaceutics* 472 (2014) 65–73. doi:10.1016/j.ijpharm.2014.05.042.
- [49] J. Enfield, M.-L. O’Connell, K. Lawlor, E. Jonathan, C. O’Mahony, M. Leahy, In-vivo dynamic characterization of microneedle skin penetration using optical coherence tomography, *Journal of Biomedical Optics* 15 (2010) 046001. doi:10.1117/1.3463002.
- 715 [50] O. Olatunji, D. B. Das, M. J. Garland, L. Belaid, R. F. Donnelly, Influence of Array Interspacing on the Force Required for Successful Microneedle Skin Penetration: Theoretical and Practical Approaches, *Journal of Pharmaceutical Sciences* 102 (2013) 1209–1221. doi:10.1002/jps.23439.
- 720 [51] J. S. Kochhar, T. C. Quek, W. J. Soon, J. Choi, S. Zou, L. Kang, Effect of Microneedle Geometry and Supporting Substrate on Microneedle Array Penetration into Skin, *Journal of Pharmaceutical Sciences* 102 (2013) 4100–4108. doi:10.1002/jps.23724.

- 725 [52] S. Verdier-Sévrain, F. Bonté, Skin hydration: A review on its molecular mechanisms, *Journal of Cosmetic Dermatology* 6 (2007) 75–82. doi:10.1111/j.1473-2165.2007.00300.x.
- [53] K. De Boulle, R. Glogau, T. Kono, M. Nathan, A. Tezel, J.-X. Roca-Martinez, S. Paliwal, D. Stroumpoulis, A Review of the Metabolism of 1,4-Butanediol Diglycidyl Ether-Crosslinked Hyaluronic Acid Dermal Fillers:, *Dermatologic Surgery* 39 (2013) 1758–1766. doi:10.1111/dsu.12301.
- 730 [54] J. Fraser, T. Laurent, Turnover and metabolism of hyaluronan, *Ciba Foundation Symposium* (1989). doi:10.1002/9780470513774.ch4.
- [55] J. R. E. Fraser, T. C. Laurent, U. B. G. Laurent, Hyaluronan: Its nature, distribution, functions and turnover, *Journal of internal medicine* 242 (1997) 27–33.
- [56] T. R.R. Singh, N. J. Dunne, E. Cunningham, R. F. Donnelly, Review of Patents on Microneedle Applicators, *Recent Patents on Drug Delivery & Formulation* 5 (2011) 11–23. doi:10.2174/187221111794109484.
- 735 [57] A. Ripolin, J. Quinn, E. Larrañeta, E. M. Vicente-Perez, J. Barry, R. F. Donnelly, Successful application of large microneedle patches by human volunteers, *International Journal of Pharmaceutics* 521 (2017) 92–101. doi:10.1016/j.ijpharm.2017.02.011.
- 740 [58] M. Leone, S. Romeijn, B. Slütter, C. O’Mahony, G. Kersten, J. A. Bouwstra, Hyaluronan molecular weight: Effects on dissolution time of dissolving microneedles in the skin and on immunogenicity of antigen, *European Journal of Pharmaceutical Sciences* 146 (2020) 105269. doi:10.1016/j.ejps.2020.105269.
- [59] Y. Chen, J. Wang, D. Flanagan, *Fundamental of Diffusion and Dissolution*, in: *Developing Solid Oral Dosage Forms*, Elsevier, 2017, pp. 253–270. doi:10.1016/B978-0-12-802447-8.00009-1.
- 745 [60] R. F. Donnelly, P. A. McCarron, J. M. Lightowler, A. D. Woolfson, Bioadhesive patch-based delivery of 5-aminolevulinic acid to the nail for photodynamic therapy of onychomycosis, *Journal of Controlled Release* 103 (2005) 381–392. doi:10.1016/j.jconrel.2004.12.005.
- 750 [61] R. F. Donnelly, P. A. McCarron, A. D. Woolfson, Drug Delivery of Aminolevulinic Acid from Topical Formulations Intended for Photodynamic Therapy, *Photochemistry and Photobiology* (2005) 750–767.

- [62] D. I. Morrow, P. A. McCarron, A. D. Woolfson, P. Juzenas, A. Juzeniene, V. Iani, J. Moan, R. F. Donnelly, Influence of penetration enhancers on topical delivery of 5-aminolevulinic acid from bioadhesive patches, *Journal of Pharmacy and Pharmacology* 62 (2010) 685–695.
- [63] P. A. McCarron, R. F. Donnelly, A. Zawislak, A. D. Woolfson, Design and evaluation of a water-soluble bioadhesive patch formulation for cutaneous delivery of 5-aminolevulinic acid to superficial neoplastic lesions, *European Journal of Pharmaceutical Sciences* 27 (2006) 268–279. doi:10.1016/j.ejps.2005.10.009.
- [64] R. Stern, Hyaluronan catabolism: A new metabolic pathway, *European journal of cell biology* 83 (2004) 317–325.
- [65] Y. Li, Q. Zhou, Z. Hu, B. Yang, Q. Li, J. Wang, J. Zheng, W. Cao, 5-Aminolevulinic Acid-Based Sonodynamic Therapy Induces the Apoptosis of Osteosarcoma in Mice, *PLOS ONE* 10 (2015) e0132074. doi:10.1371/journal.pone.0132074.
- [66] J. Dan, X. Sun, W. Li, Y. Zhang, X. Li, H. Xu, Z. Li, Z. Tian, S. Guo, J. Yao, W. Gao, Y. Tian, 5-Aminolevulinic Acid-Mediated Sonodynamic Therapy Promotes Phenotypic Switching from Dedifferentiated to Differentiated Phenotype via Reactive Oxygen Species and p38 Mitogen-Activated Protein Kinase in Vascular Smooth Muscle Cells, *Ultrasound in Medicine & Biology* 41 (2015) 1681–1689. doi:10.1016/j.ultrasmedbio.2014.12.664.

